Improving the properties of antifouling hybrid composites: The use of Halloysites as nano-containers in epoxy coatings

Colloids and Surfaces A: Physicochemical and Engineering Aspects xxx (xxxx) 126779

Contents lists available at ScienceDirect

Colloids and Surfaces A: Physicochemical and Engineering Aspects

journal homepage: www.elsevier.com/locate/colsurfa

Improving the properties of antifouling hybrid composites: The use of Halloysites as nano-containers in epoxy coatings

Monica Tonelli, Ilaria Perini, Francesca Ridi*, Piero Baglioni

Department of Chemistry "Ugo Schiff" & CSGI, University of Florence, Via della Lastruccia 3, Sesto Fiorentino, I-50019 Florence, Italy

ARTICLE INFO

Keywords:
Marine fouling
Nano-composite
Ecofriendly antifouling actives
Sodium salicylate
N-(2,4,6-trichlorophenyl)maleimide

ABSTRACT

Marine biofouling is an age-old problem with a broad impact in many marine activities. The development of environmentally friendly and long-term marine antifouling coatings remains a huge challenge in the maritime industry and involves many factors: hydrophobicity, surface roughness, electrostatic interactions, and the use of anti-adhesive/biocide molecules. We developed a novel antifouling epoxy paint doped with Halloysite clay nanotubes (HNTs) as nano-containers. HNTs were loaded with two eco-sustainable antifouling molecules, sodium salicylate and N-(2,4,6-trichlorophenyl)maleimide, which can dramatically reduce bacterial attachment. The dispersion procedure of the nano-carriers in the paint was optimized so that an efficient antifouling effect is reached with the incorporation of a small amount of loaded HNTs. The use of 10 wt% of loaded HNTs in paint drastically enhanced material antifouling properties by preventing the attachment of *Vibrio natriegens* marine bacteria, which promises wide applications for the protection of ships' hulls.

1. Introduction

Marine fouling, the process of accumulation of microorganisms, plants, algae and animals on submerged surfaces, has a devastating ecological and economic impact [1], affecting wild fisheries, aquaculture, marine sensors, shipping, and promoting corrosion phenomena [2]. To preserve as long as possible surfaces from bio deterioration, a number of strategies have been developed in the last years to fabricate coatings that resist adhesion of biocontaminants or degrade or kill them [3,4]. Among all the strategies to provide protection, researchers have found that control over hydrophobicity, surface roughness, electrostatic interactions, and the use of anti-adhesive/biocide molecules can dramatically reduce bacterial attachment [4,5]. In particular, the use of antifouling agents prevents the attachment of living organisms and the formation of biofilms, while antibacterial agents are substances capable to kill bacteria or compromise their metabolic activity, promoting an unfavorable environment for their reproduction and growth [6,7]. Typically, both these agents are used as additives to be included in protective coatings, like paints, and released over time. Over the years several antifouling paints have been synthesized and used in diverse situations to prevent marine growth [8–10]. During 1960–1970 many toxic and environmentally hazardous substances were used, such as heavy metals, arsenic and tributyl tin because of their effective biocidal properties [6,7]. Nowadays environmentally safe substances are under investigation and the emphasis is now on the use of nontoxic and/or ecofriendly materials, which do not negatively affect the environment upon application [8,11].

Antifouling agents can be also encapsulated in nano-carriers, to achieve an extended protection and avoid a potentially harmful fast release. Halloysite nanotubes (HNTs) are promising nanoclays to be incorporated in resins and paints [12,13]. HNTs are cheap and ecofriendly aluminosilicate clays with a tubular morphology exposing silica on the external surface and alumina on the inner surface, allowing for the encapsulation of active molecules to be slowly released [14,15]. In the literature, HNTs were already used as fillers for polymeric coating formulations, but the obtainment of a homogeneous dispersion is generally difficult to achieve because, in particular in epoxies, HNTs tend to agglomerate under the influence of the van der Waals forces [13], even when using small amounts of HNTs (~1 wt%) [16]. The formation of clusters and agglomerates, typically having dimensions of

Abbreviations: HNT, Halloysites; NaSA, sodium salicylate; SA-, salicylate, TCPM, N-(2,4,6-trichlorophenyl)maleimide; SEM, Scanning Electron Microscopy; TGA, thermogravimetric analysis; DSMO, dimethyl sulfoxide; AFM, Atomic Force Microscopy; BET, Brunauer-Emmett-Teller; BJH, Barrett-Joyne-Halenda; SM, Supplementary material

* Corresponding author.
E-mail address: francesca.ridi@unifi.it (F. Ridi).

https://doi.org/10.1016/j.colsurfa.2021.126779
Received 9 March 2021; Received in revised form 28 April 2021; Accepted 29 April 2021

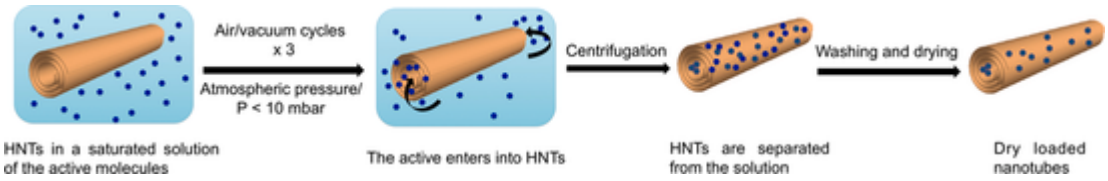

Fig. 1. Scheme of HNTs loading.

Table 1
BET surface area, total pore volume and loading weight percentages. The amount of loaded actives was calculated from TG curves by comparing the residual mass at 800 °C for SA^- and looking at the weight loss in the range 130 – 250 °C for TCPM.

Sample	BET surface area (m^2/g)	Total pore volume (mL/g)	Loading %
Pristine HNTs	26 ± 3	0.15 ± 0.02	–
Etched HNTs	34 ± 3	0.22 ± 0.02	–
Pristine HNTs loaded with SA^- in water at pH ≈ 7	18 ± 2	0.18 ± 0.02	11 ± 1
Pristine HNTs loaded with SA^- in water at pH ≈ 8 (**HNT-SA**)	18 ± 2	0.13 ± 0.01	19 ± 2
Etched HNTs loaded with SA^- in water at pH ≈ 8	18 ± 2	0.17 ± 0.02	18 ± 2
Pristine HNTs loaded with TCPM in DMSO (**HNT-TCPM**)	30 ± 3	0.34 ± 0.03	19 ± 2

tens of micrometers [17], could also adversely affect some mechanical properties (tensile, impact and flexural) [18]. To tackle the poor dispersion of HNTs in epoxy coating, a possible strategy is the functionalization of the nanotubes or the use of very small amounts of HNTs [19–24]. At the same time, a high amount of loaded nanocarriers is generally necessary to obtain an effective antifouling effect [13,16,17].

Another approach to reduce marine fouling consists in the use of rough surfaces, that are able to reduce the attachment of organisms by displaying a smaller contact area and eventually inducing a deformation of the bacteria cell membrane [25–28]. Both coatings' composition and particular surface morphology can be matched to provide effective antifouling properties [29].

In this work, we prepared a hybrid composite made of an epoxy paint enhanced with HNTs loaded with two different molecules, not hazardous for the environment: sodium salicylate (NaSA), a biocide molecule, and *N*-(2,4,6-trichlorophenyl)maleimide (TCPM), an anti-adhesive molecule [30–32]. To this purpose, we selected a commercial epoxy paint, specifically formulated for the protection of ships' hulls. First, the loading procedure for NaSA and TCPM in HNTs was optimized. Then, we fine-tuned a procedure able to produce a homogeneous dispersion of 10 wt% HNTs in the epoxy coating, with no need of superficial functionalization. In the previous literature a much higher amount of loaded HNTs (22 wt% [14] or 28 wt%[31]) was necessary in analogous systems for allowing the obtainment of a good inhibition of bacteria attachment. Here, the optimization of the dispersion method produced an effective antifouling efficacy using only 10 wt% of HNTs. This is an important achievement as it implies the reduction of the costs associated to the use of expensive environmentally-safe actives.

The composites were fully characterized to evaluate the effect of the incorporation of HNTs into the paint, especially in terms of roughness and wettability. The antifouling properties of the composites were tested by monitoring the surface adhesion and proliferation of marine *Vibrio natriegens* bacteria with Scanning Electron Microscopy (SEM). *V. natriegens* is a widely diffused gram-negative marine azotobacter, which adsorbs on structures immersed in sea and forms a biofilm on the surface, providing the ideal conditions for the adhesion of other sea creatures [31]. By monitoring the kinetics of release of the two investigated antifouling agents from the composites, it appears that the antifouling effect is obtained with the release of very low amounts of active molecules in water, which is an advantage, from an environmental point of view, even when using non-hazardous molecules. According to the results, a significant quantity of actives remains stuck in the epoxy paint and is not released in water, but the presence of these trapped molecules allows for a prolonged protection of the surface exposed to marine fouling, and preserves it from bio deterioration.

2. Experimental

2.1. Materials

Halloysite nanoclays (density 2.55 g/cm^3 as from technical datasheet, length of 0.5–2 μm as from SEM images, specific surface area measured by means of a Coulter SA 3100 analyzer = 26 m^2/g) were obtained from Imerys, sodium salicylate (NaSA, purity 99.5%) was purchased from Sigma-Aldrich, N-(2,4,6- trichlorophenyl) maleimide (TCPM, purity 98%) from Combi-Blocks, sulfuric acid (purity 96%) from Carlo Erba, NaOH from Sigma-Aldrich and dimethyl sulfoxide (DMSO, 0.03% water) from Merck. The two-component epoxy coating Penguard HB red was purchased from Jotun.

2.2. Preparation of antifouling HNTs

2.2.1. Etching of HNTs

Following a procedure already reported in the literature for the etching treatment [32], a suspension of 5 g of HNTs in 500 mL of a 2 M H_2SO_4 water solution was kept under magnetic stirring at 25 °C for 48 h. Then, HNTs were filtered with a cellulose nitrate filter (cut-off 0.1 μm), repeatedly washed with Milli-Q water and separated by centrifugation, until a pH ≈ 6 was reached. Etched HNTs were dried at 70 °C and characterized by SEM images and nitrogen adsorption/desorption isotherms to evaluate the efficacy of the etching treatment.

2.2.2. Loading of HNTs with SA^-

HNTs were loaded with salicylate (SA^-) by adding 2 g of pristine HNTs or etched HNTs in a saturated solution of NaSA in water (≈ 1.17 g/mL, 22 g NaSA in 20 mL H_2O) under magnetic stirring, adjusting the pH at 8 with NaOH 1 M and repeating cycles of vacuum/air. The suspension was evacuated with a vacuum pump for about 30 min and sealed to maintain the vacuum for 1 h while monitoring the pressure, which never exceeded 10 mbar. The suspension was evacuated with a vacuum pump for 30 more minutes and then cycled back to atmospheric pressure for 1 h. Then, it was evacuated again for 1 h at P < 10 mbar and placed at atmospheric pressure for 1 h. The air/vacuum procedure was repeated up to 4 times to evaluate the ideal number of cycles: after every cycle, a small aliquot was withdrawn, centrifuged, rapidly washed with 10 mL of Milli-Q water and dried at 70 °C. The samples (HNT-SA) were characterized through SEM, thermogravimetric analysis (TGA) and nitrogen adsorption/desorption analysis.

2.2.3. Loading of HNTs with TCPM

According to the literature [31], HNTs can be loaded with TCPM in water solution at 2:1 HNT:TCPM ratio, by mixing HNTs (100 g/L) with TCPM (50 g/L) and repeating three vacuum/air cycles. Following

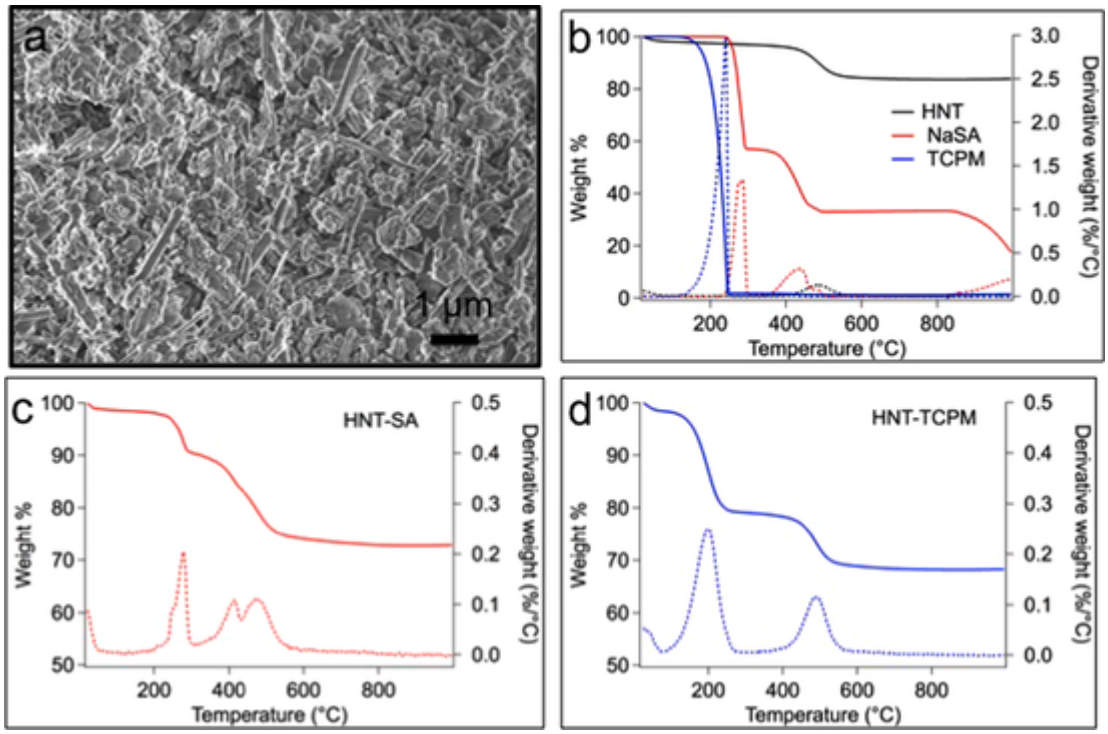

Fig. 2. SEM image of pristine HNTs Imerys (a); TG curves of pristine HNTs, SA and TCPM (b), HNTs loaded with SA in water at pH ≈ 8 (c), and HNTs loaded with TCPM in DMSO (d).

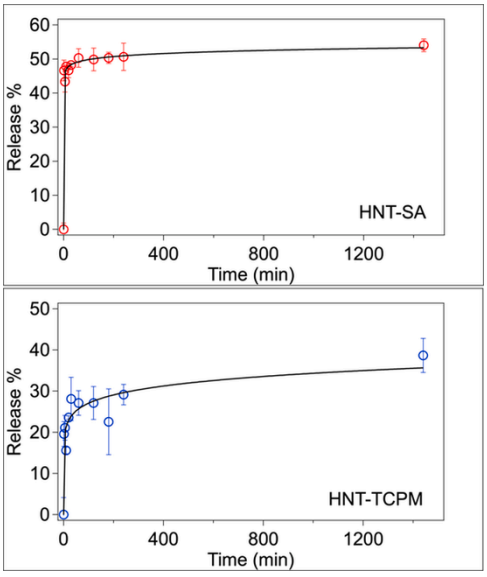

Fig. 3. Release kinetic profiles of SA^- and TCPM from HNTs. Markers represent the average calculated on 3 experimental measurements ± standard deviation; the corresponding fitting curves were calculated according to Korsmeyer-Peppas equation.

the paper by Fu et al. [31], we prepared a suspension of 5 g of pristine HNTs and 2.5 g of TCPM in 50 mL of water, using the same loading procedure of vacuum/air cycles described in the previous section. We observed the presence of abundant insolubilized TCPM in solution and we found that the recommended concentration is way above the solubility of TCPM in water at 25 °C, that we found to be 0.01 g/L.

Thus, we used a different solvent to load TCPM in HNTs, DMSO, to avoid the presence of insolubilized TCPM. 3.4 g HNTs were mixed in a saturated solution of TCPM in DMSO (≈ 0.36 g/mL, 5.1 g TCPM, 14 mL DMSO) and we used the same loading procedure described in Section 2.2.2. When necessary, we refilled the solvent eventually evaporated during the vacuum cycles. After the last cycle, HNTs were separated by centrifugation, washed with 12 mL of DMSO once and with 12 mL Milli-Q water four times, and dried at 70 °C. The samples (HNT-TCPM) were characterized through SEM, TGA and nitrogen adsorption/desorption isotherms.

2.3. Preparation of the composites

The epoxy paint Penguard HB was prepared by mixing two components, Comp A and Comp B at 4:1 vol ratio. Penguard HB Comp A contains the epoxy resin and Penguard Comp B is the amide-based curing agent [33]. HNTs were incorporated in Comp A, to achieve a weight percentage of 10% of nanotubes in the final composite (4 mL Comp A + 1 mL Comp B). HNTs were mechanically mixed with a spatula for 5 min and with a vortex for 3 min and sonicated for 30 min at 30 °C and 59 Hz. This procedure was repeated 3 times to achieve a homogeneous dispersion of HNTs in Comp A. Then, Comp B was added, the paint was again mechanically mixed 5 min with a spatula and 3 min with a vortex, and sonicated 30 min. To spread the films, the paint was poured on smooth plastic sheets and rolled with a Metering Rod from GARDCO (Paul N. Gardner Company Inc.), with a wire size of 44, corresponding to a final thickness of the film of 112.8 μm. The composites were allowed to air-dry overnight and characterized through SEM and Atomic Force Microscopy (AFM). For the study of the kinetics of release we prepared HNT-SA/paint, HNT-TCPM/paint and also SA/paint and TCPM/paint, where NaSA and TCPM were directly incorporated into the epoxy paint, to gain information on the advantages of using HNT nanotubes as nano-carriers for a slow delivery of active molecules.

2.4. Methods

2.4.1. Characterization

SEM was performed on a ΣIGMA Field Emission SEM (Carl Zeiss Microscopy GmbH, Germany), using an InLens detector. The used accelerating potential was 2 kV for the morphological characterization of

Table 2
Results of the curves of release fitted according to Korsmeyer-Peppas model.

	k_{KP}	n_{KP}	Chi-square
HNT-SA	0.83 ± 0.02	0.016 ± 0.006	24
HNT-TCPM	0.45 ± 0.01	0.089 ± 0.007	94
HNT-SA/paint	0.21 ± 0.06	0.27 ± 0.06	2
SA/paint	0.20 ± 0.04	0.30 ± 0.04	6
HNT-TCPM/paint	0.15 ± 0.06	0.34 ± 0.08	2

HNTs powders, and 1 kV for the characterization of the dried paint/HNTs composites.

The Specific Surface Area and Pore Size Distribution of pristine, etched and loaded HNTs were measured by means of a Coulter SA 3100 analyzer (Beckman Coulter), using nitrogen as adsorptive gas. Before the measurements, the dried samples were outgassed for 90 min at 50 °C. Brunauer-Emmett-Teller (BET) [34] and Barrett-Joyne-Halenda (BJH) [35] calculations were used respectively for the analyses of specific surface area and pore volume data.

Thermogravimetric analysis of pure NaSA, pure TCPM, pristine, etched or loaded HNTs was conducted on a SDT Q600 (TA Instruments, Philadelphia, PA, USA) in N_2 atmosphere (flow rate 100 mL/min) from room temperature to 1000 °C at 10 °C/min under nitrogen flow.

AFM was performed with a Park System XE-7 microscope equipped with NCHR probes (radius of curvature < 10 nm) in non-contact mode. Calculation of the roughness parameters and image processing were performed using the Park Systems XEI software 1.8.2.

Static contact angle of water was measured (KSV Cam 200) on paint and HNT/paint composites. The reported water static contact angle values are the average of at least 9 droplets of 10 μL on different regions of 3 specimens.

Dynamic contact angle of water was measured by means of a K100 Force Tensiometer Krüss GmbH on paint and HNT/paint composites. Two specimens were tested for each sample by measuring the advancing and receding contact angles of pristine films immersed in MilliQ water at 25 °C. Films were immersed/withdrawn during 6 consecutive cycles, with a speed of 1 mm min^{-1}, minimum and maximum immersion depths of 1 and 5 mm, respectively. Contact angle values were estimated through the Krüss Laboratory Desktop software, version 3.2, as the results of a linear regression of the force versus position graph. The regression was calculated in the linear region of the graph for each cycle (both advancing and receding), taking into account width and thickness of films. Data are reported as mean value ± standard deviation over all the cycles.

2.4.2. Release kinetic

The amount of released SA^- or TCPM was quantified by means of UV spectroscopy. Samples were analyzed in quartz cuvettes with a

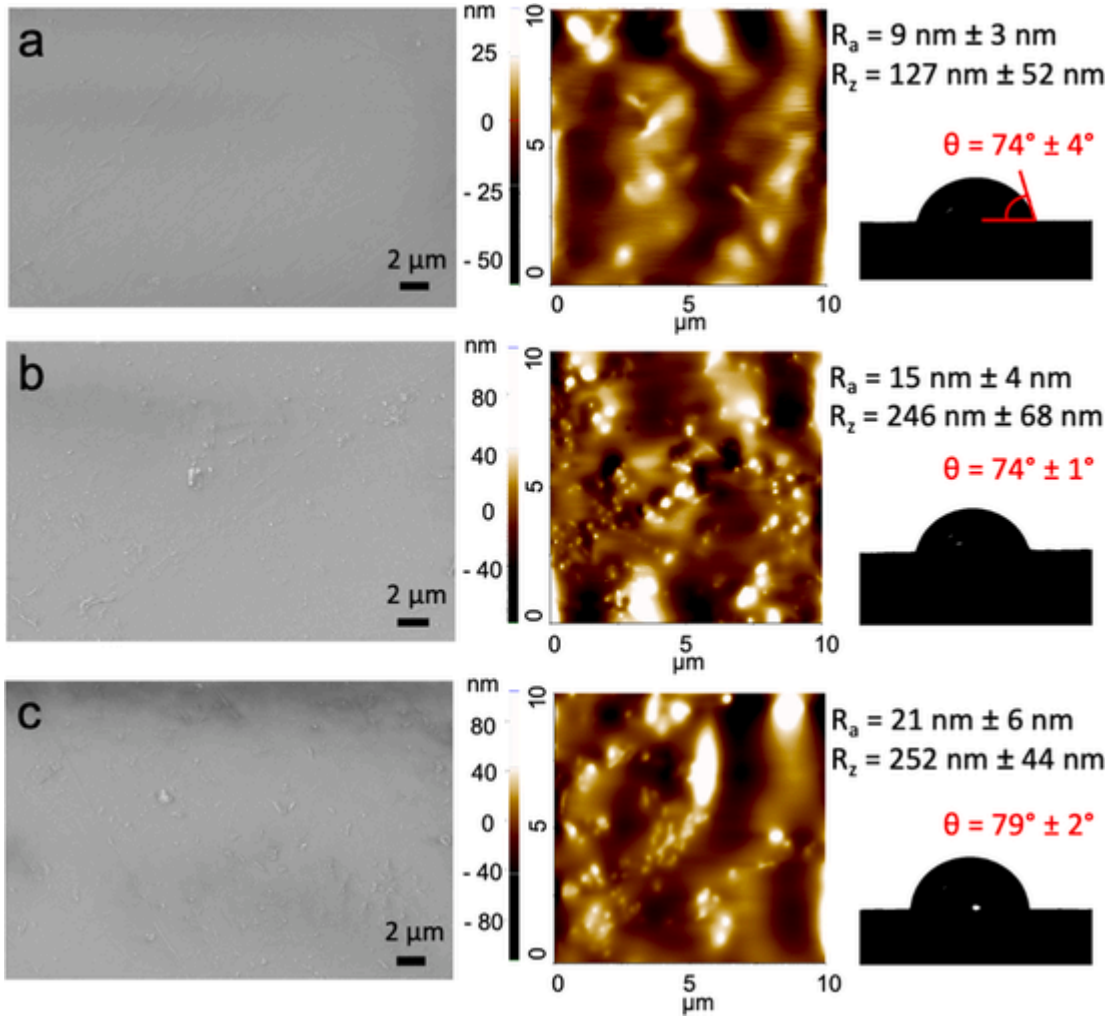

Fig. 4. SEM and AFM images of pristine paint (a); HNT-SA/paint and (b); HNT-TCPM/paint coatings (c) with the corresponding optical micrographs of water contact angle. The reported roughness values are the average of 3 maps acquired on different regions of the samples. The reported water static contact angle values are the average of at least 9 droplets placed on different regions of 3 specimens.

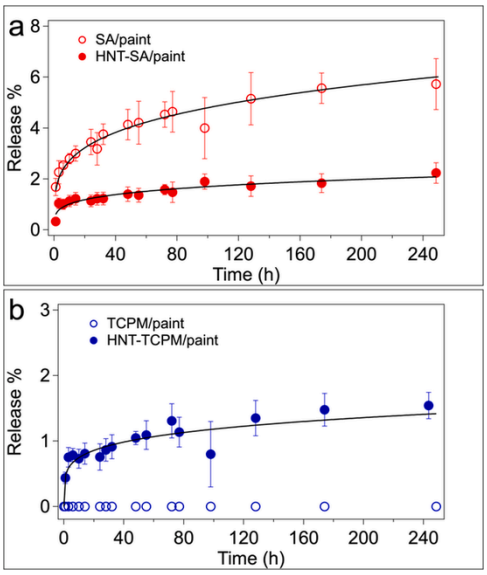

Fig. 5. Release kinetic profiles of SA^- (a) and TCPM (b) from the composites. Markers represent the average calculated on 3 experimental measurements ± standard deviation; the corresponding fitting curves were calculated according to Korsmeyer-Peppas equation.

Cary3500 (Agilent) in the range 190–400 nm, with an integration time of 0.5 s and a bandwidth of 1 nm. Prior to the measurement, calibration lines of NaSA and TCPM in water were acquired: the absorbance of NaSA was measured at 296 nm and we found that A = 0.033·c – 0.013, where c is the concentration of NaSA (μg/mL); while the absorbance of TCPM was measured at 207 nm and we found that A = 0.16·c + 0.032.

Two methods were used to evaluate the kinetic of release of SA^- from HNTs. In the first method, HNT-SA were mixed in Milli-Q water (15 mg in 100 mL) and kept under magnetic stirring at 25 °C in a thermostatic water bath. At predetermined times we collected ~1 mL of suspension, which was filtered with a 0.22 μm hydrophilic syringe filter. The concentration of SA^- released at each withdrawal was quantified by means of UV–vis analyses. In the second approach, 10 mg of HNT-SA were added in 5 mL of water and kept under magnetic stirring at 25 °C. At predetermined times we collected 50 μL of suspension, which was diluted with 450 μL of water and centrifuged (12,000 rpm, 5 min). At each withdrawal, 50 μL of water was added to the suspension to replace the withdrawn volume. The concentration of the released SA^- was quantified by measuring the absorbance of the supernatant separated from the centrifugation. The release of TCPM from HNT-TCPM was studied through the second method.

To investigate the release kinetic of SA^- and TCPM from the HNT/paint composite, a 5 × 5 cm^2 film containing 10 wt% of loaded HNTs was added to 5 mL of Milli-Q water, continuously stirred (130 rpm) and kept at 25 °C. At predetermined times 50 μL of suspension was withdrawn and replaced with 50 μL of water. The withdrawal was diluted with 450 μL of water and analyzed by UV–vis spectroscopy to quantify the amount of released SA^- or TCPM.

A quantitative evaluation of the release properties was obtained by fitting the experimental data according to some of the most commonly used models in the analysis of drug-released molecules, reporting the released amount of drug as the ratio between the cumulative amount of drug released at time t, M_t, and infinite time, M_∞ (M_t/M_∞). In the Higuchi equation [36], the fractional release M_t/M_∞ is proportional to the square root of time

$$\frac{M_t}{M_\infty} = k_H t^{1/2} \quad (1)$$

where k_H is the dissolution factor. In the Korsmeyer-Peppas equation [37–39].

$$\frac{M_t}{M_\infty} = k_{KP} t^{n_{KP}} \quad (2)$$

where k_{KP} accounts for the structure and geometry of the dosage form, while n_{KP} is used to characterize different transport mechanisms: $n_{KP} \leq 0.5$ corresponds to a Fickian transport, $0.5 < n_{KP} < 1$ corresponds to non Fickian transport, $n_{KP} = 1$ to Case-II transport, and $n_{KP} > 1$ to super Case-II transport. In Weibull model [40,41].

$$\frac{M_t}{M_\infty} = 1 - \exp(-k_W t^{n_W}) \quad (3)$$

where k_W defines the time scale of the process, and n_W is used to indicate the transport mechanism: $n_W \leq 0.75$ corresponds to a Fickian transport, $0.75 < n_W < 1$ indicates a combination of Fickian diffusion and Case-II transport, $n_W > 1$ indicates a complex transport mechanism.

2.4.3. Antifouling assay

Vibrio natriegens (*V. natriegens* DSM 759) ATCC 14048 was purchased from DSMZ and used as a model strain to investigate the antifouling ability of the composites. *V. natriegens* was grown overnight in nutrient broth (4.5 g tryptic soy broth from Aldrich, 1.5 g NaCl from Sigma Aldrich and 150 mL Milli-Q H_2O) at 30 °C. Samples with the size of 1.2 cm diameter were hung in the bacterial suspension (OD600 nm = 1.0) and incubated for 7 days at 30 °C. Then the surfaces were rapidly washed two times with 5 mL artificial seawater (prepared according to Zakowski et al. [42].) and fixed with glutaraldehyde. After a 4 h fixation in 2.5% glutaraldehyde, the samples were washed two times with 5 mL artificial seawater and progressively dehydrated in 60%, 70%, 80%, 90% and 99.2%, ethanol solutions for 10 min each. Afterwards, they were freeze-dried for 4 h, attached on stubs, coated with a gold film with a JEOL Jee 4B apparatus and observed by means of SEM using an InLens detector and an accelerating potential of 2 kV. ImageJ was used to calculate the area covered by bacteria by looking at the SEM images acquired at 3 KX. The reported percentages of coverage are the average the measurements calculated on 5 different regions of the surfaces.

3. Results and discussion

3.1. Optimization of the loading in HNTs

In this study, we started with the optimization of the loading procedure for the selected molecules (see the scheme in Fig. 1). In order to have abundant solubilized active molecules, we used water and DMSO for the loading of NaSA and TCPM, respectively. As very recently reported by Lisuzzo et al. [43], one of the driving forces for a successful loading of HNTs is the use of a very low pressure, like the one used in this work (P < 10 mbar). Lisuzzo et al. [43]. reported that when applying vacuum to a suspension of Halloysites, once the vapor pressure of the solvent is approached, it starts to evaporate and the molecules confined in the cavities of the nanotube evaporate faster than the bulk ones. This generates an enrichment of active molecules (that were dispersed in the solvent) into the lumen, favoring the encapsulation. The presence of molecules weakly adsorbed outside HNTs cannot be ruled out, but, for the purposes of our study, this would not negatively affect the HNTs' role as "collectors" and carriers. According to literature, the maximum loading capacity for pristine HNTs is about 10 wt% [44], but the loading capacity of HNTs could be also increased up to 4 times with a selective etching of the alumina sheets of the inner hollow tube, the lumen, to enlarge the cavities.

At the same time, it was already reported in the literature that a slightly basic pH maximizes the negative charge of salicylate, while the

Table 3
Static and dynamic water contact angles measured on the pristine paint, HNT-SA/paint and HNT-TCPM/paint composites. The results are reported as average ± standard deviations.

	Pristine paint	HNT-SA/paint	HNT-TCPM/paint
Advancing contact angle	82 ± 2	79 ± 2	87 ± 1
Receding contact angle	20 ± 3	23 ± 6	23 ± 3
Hysteresis	63 ± 2	55 ± 6	64 ± 3

inner alumina surface of HNTs remains positively charged up to pH 8.5 [32,45,46]. By looking at the amount of loaded SA^- in etched HNTs and in HNTs loaded at pH ≈ 8, we can evaluate the effect of the lumen enlargement and that of the maximization of the attractive forces between SA^- and HNTs' inner surface. The surface area and pore volume of these samples are reported in Table 1, together with the amount of loaded actives, calculated from the TG curves. As expected, the etching treatment increased the BET surface area and total pore volume and favored the loading (loading ≈ 18%), but with pristine HNTs loaded at pH ≈ 8 we obtained the same loading efficacy (loading ≈ 19%). Fig. 2 shows the SEM image of HNTs (Fig. 2a), together with the thermogravimetric (TG) curves of the pristine reactants (Fig. 2b), HNTs, not etched, loaded with SA^- at pH ≈ 8, HNT-SA (Fig. 2c), and HNTs loaded with TCPM in DMSO (Fig. 2d). Fig. S1 (see the Supplementary material, SM) reports the SEM images of pristine and etched HNTs together with their adsorption isotherms and pore volume distribution, and TG curves before and after the loading at pH = 7 and pH = 8. We did not observe differences in terms of morphology before and after the etching treatment, but the surface area was increased, as expected. We confirmed that SA^- was loaded into HNTs' cavities in all cases and the loading was more efficient at pH 8, for both pristine and etched HNTs. We found that a slightly basic pH of the solution, maximizing the electrostatic attractive forces between SA^- and HNTs' lumen, increased the loading more than the enlargement of the lumen obtained by etching treatment.

Thus, since the etching treatment may affect the mechanical properties of the tubules [32], a loading procedure on pristine HNTs in slightly basic conditions was preferred. In general, when possible, it seems preferable to choose electrostatic attraction as the driving force of the loading, by properly maximizing the interaction between the active molecules and the cavities of HNTs, rather than using time-consuming and potentially harmful treatments. In order to evaluate also the ideal number of air/vacuum cycles, HNT-SA aliquots were withdrawn after each cycle and the amount of loaded SA^- was quantified through TGA (see Fig. S2 in the SM). According to the results, the amount of loaded SA^- increased in the first 3 cycles and then remained constant, indicating that 3 cycles are sufficient to reach the maximum loading.

Following the procedure described in Section 2.2.3 and reported in Fig. 1, HNT-TCPM were prepared in a solvent where abundant quantities of TCPM might be dissolved, DMSO, and the successful loading was confirmed by TGA (see Fig. 2d). The amount of loaded TCPM was ≈ 19%, as reported in Table 1. When loading TCPM we can observe an increase of the BET surface area and total pore volume. It might be possible that DMSO interacts with HNTs, since in the literature it was suggested that this solvent could intercalate kaolin minerals [47].

3.2. Release kinetics of the antifoulants from HNTs

The kinetic of release of SA^- and TCPM was first studied from HNTs powders in water. The first method described in Section 2.4.2 for HNT-SA consists in filtering the collected withdrawals and initially seemed to give satisfactory results, since we observed an increase with time of SA^- absorbance (see Fig. S3a, SM). By closely looking at the spectra acquired at different times (Fig. S3b, SM) we noticed that the baseline was actually increasing, influencing the value of absorbance measured at 296 nm for SA^-. We ascribed the increase that we observed in the baseline to scattering phenomena arising from HNTs, implying that the filter was unable to completely separate the contribute of HNTs from the one arising from the active molecules. A deconvolution of the signals (Fig. S3d, SM) allowed the separation of SA^- contribute from HNT contribute and we found that SA^- absorbance remained almost constant starting from 3 min, while the scattering contribution assigned to the growing amount of HNTs' fragments increased. Thus, it seems very important to take into account possible HNTs' contributes when studying kinetics of release from HNTs, as they might lead to incorrect results.

A second method described in Section 2.4.2 was then used to study the kinetics of HNT-SA and HNT-TCPM, as reported in Fig. 3. Following this method, by separating HNTs through centrifugation, we observed a constant baseline without scattering noise. A quantitative evaluation of the release properties can be obtained by fitting the experimental data according to some of the most commonly used models in the analysis of drug-released molecules [48]. Here we tested the model by Higuchi [36], Korsmeyer-Peppas [37–39] and Weibul [40,41]. The goodness of each fitting was evaluated in terms of chi-square and we found that in both cases Korsmeyer-Peppas equation ($M_t/M_\infty = k_{KP}t^{n_{KP}}$, where M_t is the amount of drug released at time t, M_∞ is the amount of drug released at infinite time, n_{KP} is the exponent characteristic of the release mechanism, and k_{KP} is a constant) accurately accounts for the release process. The results of the fittings are reported in Table 2. According to the results, $n_{KP} < 0.5$ for both kinetics (see Table 2), indicating that the release of antifoulant from HNTs takes place through Fickian diffusion mechanism. It was already reported in the literature that the kinetic of release of molecules confined into HNTs' lumen shows a good correlation with Korsmeyer-Peppas model, meaning that the mechanisms ruling the release of drugs from loaded halloysite is diffusion controlled [49,50].

The release of SA^- started immediately after mixing and occurred in about 1 h, while TCPM reached the plateau in about 4 h. The very fast release of SA^- can be attributed to its highly hydrophilic nature. The amount of released SA^- with respect to the maximum releasable amount (found through TGA) was about 50%, while the amount of released TCPM with respect to the maximum releasable amount was about 40%. Thus, even at the plateau some of the loaded active molecules remain bonded in the lumen and cannot be released. This was not unexpected, as it was already reported in the literature that, even at plateau, in most cases not all molecules are released from the lumen of HNTs [31,51–55].

3.3. Characterization of the composites

The dispersion of nanotubes into the paint was evaluated during the mixing procedure by eye, and after the preparation of a spread film of the paint by means of SEM, to discard the formation of agglomerates/clusters, that would have dimensions of tens of micrometers [17]. Fig. 4 (images on the left) shows the morphology of the paint (Fig. 4a, left) and of the HNT-SA/paint and HNT-TCPM/paint composites (Fig. 4b and c, left). It is possible to recognize some HNTs with random orientations in Fig. 4(b) and (c), but no agglomerates were found when scanning the samples, suggesting that the nanotubes are well dispersed in the paint. This is an important achievement, considering the difficulties often reported in the literature to obtain a homogeneous dispersion of inorganic fillers in epoxy resins [13,16–18].

In order to gain information also on the effect of HNTs on the roughness of the surface of the paint, we performed an AFM analysis, and since a nanoscale roughness is a fundamental factor when designing a surface with anti-adhesion properties, we acquired also water static contact angle measurements. Fig. 4 (images in the center) shows the maps collected on pristine paint, HNT-SA/paint and HNT-TCPM/paint, together with optical micrographs showing water static

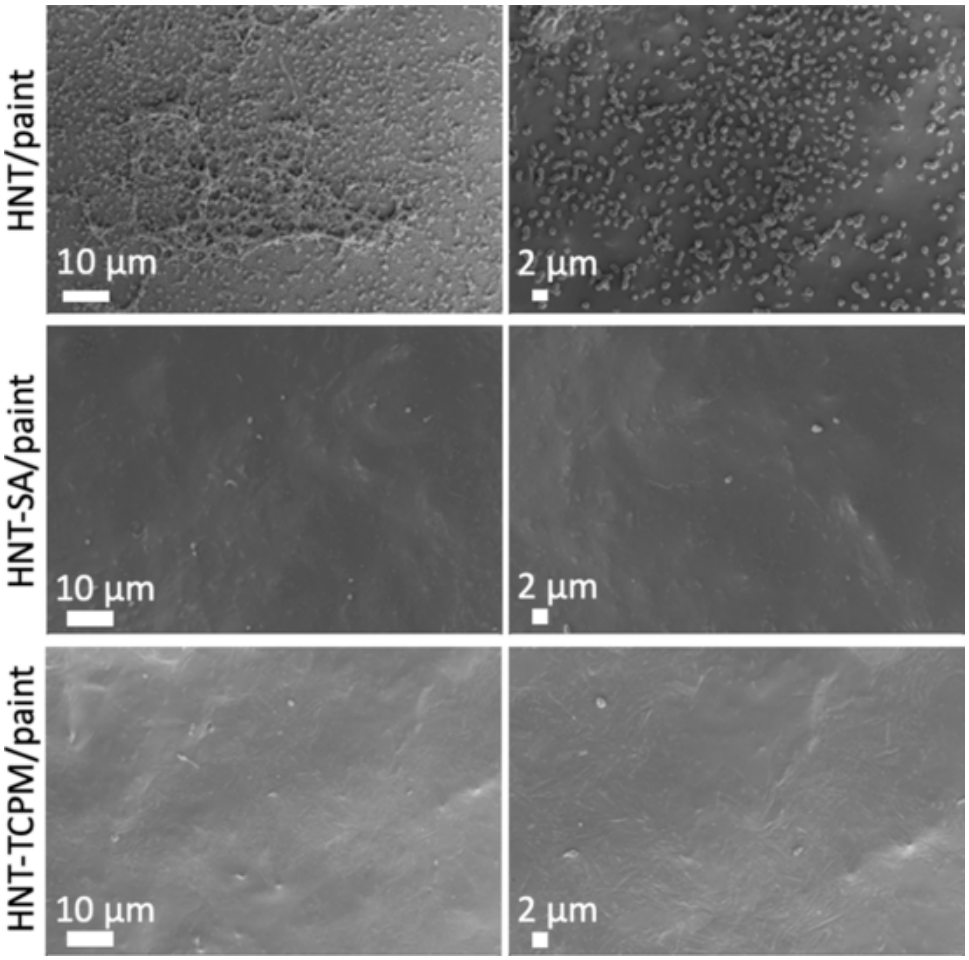

Fig. 6. SEM images of the bacteria on the surfaces.

contact angle on the corresponding surfaces (images on the right). The roughness parameters reported in Fig. 5 were calculated using the Park Systems XEI software. The roughness Ra, defined as the area between the roughness profile and its mean line, is a universally recognized parameter. According to the literature [56], the most proper roughness calculation in order to compare surfaces with different type of roughness, is the parameter Rz, which is defined as the arithmetic average of the height differences between the five highest peaks and the five lowest valleys measured over the scan length of the selected area. In Fig. 5 we reported both Ra and Rz. Based on the results, HNTs increase the roughness of the surfaces, affecting the contact area for the attachment of bacteria. Concerning the wettability, in presence of HNT-SA the wettability was unchanged, probably because of the highly hydrophilic nature of salicylate. On the opposite, HNT-TCPM/paint shows the higher water contact angle, ascribed to both the increased roughness and the hydrophobic nature of TCPM.

The measurement of the advancing and receding contact angles enabled us to provide more information on the surfaces of the investigated systems. The registered advancing-receding contact angle vs position curves (see Table 3 and Fig. S4) show a large hysteresis for all the investigated samples. In the literature, such large values of hysteresis have been associated with high values of roughness of the surfaces [57], even though some other factors can affect its extent, such as chemical modifications [58], surface swelling [59], sorption effects [60]. It is worth to note, however, that the HNT-SA/paint system displays the lowest value of hysteresis, due to the lowest value of the advancing contact angle with respect to the other two systems: according to the literature [58] this effect can be associated with the presence of SA^- molecules, which introduces hydrophilic moieties on the surface.

3.4. Release kinetics of the antifoulants from the composites

The kinetics of release of SA^- and TCPM from the composites are reported in Fig. 5. Similar to what reported for the kinetics of release of the antifoulants from HNTs lumen (Section 3.2), we tested three fitting models: Higuchi, Korsmeyer-Peppas and Weibul. The goodness of each fitting was evaluated in terms of chi-square and we found that Korsmeyer-Peppas' model accurately describes all the curves, except for TCPM/paint composite, where no release was observed. The results of the fittings are reported in Table 2. The values obtained for the transport exponent n_{KP} are always < 0.5, indicating that the release of antifoulant in SA/paint, HNT-SA/paint and HNT-TCPM/paint composites takes place through Fickian diffusion mechanism, in agreement with previous reports on other polymer/drug-loaded HNT composites [50,51,61]. The release of drugs from polymeric matrices is generally driven by solute diffusion, polymeric matrix swelling, and material degradation, and it is well described by the Fick's law of diffusion. Specifically, a Fickian diffusion mechanism refers to the solute transport process in which the polymer relaxation time is much greater than the characteristic solvent diffusion time [61]. The comparison between the values of the transport constants k_{KP} indicates that the release process is slower from the composites HNT-SA/paint and HNT-TCPM/paint, than from the systems HNT-SA and HNT-TCPM. Furthermore, it can be noted that the values of k_{KP} for the HNT-SA/paint system is equal to that of SA/paint: this indicates that the diffusion through the epoxy matrix is the rate-determining process in the SA^- release. The extent of the release, however, is different (see Fig. 5a): in both cases, the profile shows a relatively rapid initial growth and then keeps on increasing gently in the following 10 days. The relative

Table 4
Percentages of fouling surface coverage (%) ± standard deviations calculated on 5 different regions of the surfaces. Percentages of coverage were calculated on SEM images acquired at 3 KX using ImageJ program.

HNT/paint	HNT-SA/paint	HNT-TCPM/paint
38 ± 11	0.50 ± 0.57	0.14 ± 0.10

amount of released SA^- estimated after 10 days is ~ 6 wt% in SA/paint and ~ 2 wt% in HNT-SA/paint composites. Thus, it can be concluded that in the composite HNTs contribute to inhibit the release process of SA^- molecules, which occurs more gradually than in the SA/paint system. Fig. 5(b) shows the kinetic profiles of the composites HNT-TCPM/paint and TCPM/paint. In this case we can see that when using TCPM directly dispersed into the paint, no release occurs, probably due to the strong affinity of the active molecules with the epoxy paint. On the other hand, when TCPM is loaded into HNTs, we observe a definite profile of release, which increases slowly during the first 10 days. This is probably due to the fact that a fraction of loaded HNTs is exposed on the paint surface, thus facilitating the withdrawal of TCPM from the matrix. The presence of other loaded HNTs inside the epoxy matrix will thus represent a reservoir of antifouling molecules, which would come into plays once the paint wear during the time consumes the surface layers or produce cracks. The relative amount of released TCPM after 10 days is about 1.5 wt% in HNT-TCPM/paint. Even if both the composites show a quite low final drug release, this is in agreement with the results reported by other papers in literature dealing with HNTs as drug delivery systems [52,62,63], and it is worth to note that such low released amounts are enough to provide the antifouling effect (see the paragraph 3.5).

3.5. Antifouling assay

To analyze the antifouling properties of HNTs/paint composites, *V. natriegens* marine bacteria was cultured on the composite surfaces and fixed, prior SEM monitoring. Fig. 6 shows the SEM images of HNT/paint, HNT-SA/paint and HNT-TCPM/paint. Looking at the images, very few bacteria can be found on the surface of the composites when HNT-SA or HNT-TCPM are present, while many bacteria are attached to the HNT/paint sample, and a biofilm is clearly forming on the surface of the pristine paint (see Fig. 6, images on the top). Table 4 reports a quantification of the surface fouling calculated as percentage of coverage of the bacteria on the different surfaces. According to the results, after 7 days of incubation about 38% of the total exposed surface of HNT/paint composite is covered by bacteria, while less than 1% of the surfaces of HNT-SA/paint and HNT-TCPM/paint composites are attached by the bacteria. It has been reported that HNTs inclusion in composites, increasing the surface roughness, might lead to better proliferation of bacteria [64], but in presence of antifouling molecules loaded into HNTs we observed that the formation of a biofilm is prevented and the surface results better protected from the accumulation of organisms. The results here presented evidence that the inclusion of 10 wt% of loaded HNTs strongly inhibits the attachment of *V. natriegens* bacteria and allows for a significant reduction of the fouling adhesion on these composites. As a comparison, according to the literature polymers doped with much higher amounts of HNTs loaded with antifoulants (e.g., 22 wt% in Ref. [14,28 wt% HNTs in Ref. [31]), show analogous enhanced antifouling properties, while here it was sufficient to use 10 wt% of HNT-TCPM or HNT-SA to drastically reduce the accumulation of bacteria on the surface. As far as we know, polymeric systems containing lower percentages (~ 2 wt%) of drug-loaded HNTs with efficient antibacterial/antifouling properties were reported only for filtration membranes [65,66]. The use of small amounts of HNTs to provide antifouling properties in paint would result in multiple advantages: i) the possibility of dispersing pristine HNTs in epoxy coating without the need of expensive and time-consuming functionalization of the nanotubes; ii) the consume of a lower amount of expensive green antifouling agents; iii) the prevention of formation of aggregates, that would negatively affect the efficacy of the antifouling effect and would worsen the mechanical properties of the composite.

4. Conclusions

We have developed a novel marine antifouling paint by doping an epoxy paint with sodium salicylate or N-(2,4,6-trichlorophenyl) maleimide loaded into Halloysite lumen. The encapsulation of SA^- and TCPM in HNTs was optimized, to achieve a loading of about 19 wt% in both cases. The highest loading capacity was obtained by properly tuning the electrostatic interaction between the cavities of HNTs and the active molecules and by choosing a solvent where abundant quantities of active molecules might be dissolved. A homogeneous dispersion of HNTs in an epoxy paint, specifically formulated for the protection of ships' hulls, was achieved combining a mechanical mixing with vortex and sonication. The dispersion protocol presented in this work enabled the obtainment of a homogeneous dispersion of 10 wt% HNTs, without needing to functionalize the nanotubes' surface. HNTs were used as nano-containers to encapsulate and extend the release of the antifouling molecules over time. In the composite, the release of antifouling agents from HNTs into water is very slow and most of the active molecules remain trapped into the matrix, prolonging the protective effect against marine fouling. Antifouling tests performed on the epoxy composites including HNT-SA or HNT-TCPM showed that the low and continuous release of actives is sufficient to prevent the attachment of *V. natriegens* marine bacteria, which instead proliferates on the surface of the pristine paint.

The results presented in this work suggest that the optimization of the loading procedure of the actives in HNTs and of the dispersion protocol of the nanotubes in the composite are fundamental for the obtainment of efficient antifouling systems.

CRediT authorship contribution statement

Monica Tonelli: Conceptualization, Investigation, Data curation, Writing - original draft, Writing - review & editing. **Ilaria Perini:** Investigation, Data curation, Writing - review & editing. **Francesca Ridi:** Conceptualization, Formal analysis, Supervision, Writing - review & editing. **Piero Baglioni:** Funding acquisition, Supervision, Writing - review & editing.

Declaration of Competing Interest

The authors declare that they have no known competing financial interests or personal relationships that could have appeared to influence the work reported in this paper.

Acknowledgements

This research was funded by H2020, InnovaConcrete Project, grant Agreement number 760858. The CSGI Consortium and MIUR-Italy ("Progetto Dipartimenti di Eccellenza 2018–2022" allocated to Department of Chemistry "Ugo Schiff") are gratefully acknowledged for financial support. Dr. Silvia Tilli and Dr. Demetrio Randazzo (Laboratorio Biologico Dipartimentale) are gratefully acknowledged for their technical support with the biological experiments.

Appendix A. Supporting information

Supplementary data associated with this article can be found in the online version at doi:10.1016/j.colsurfa.2021.126779.

References

[1] J. Aizenberg, Slippery liquid-infused porous, Surf. J. Ocean Technol. 9 (2014) 113–114.

[2] C.S. Ware, T. Smith-Palmer, S. Peppou-Chapman, L.R.J. Scarratt, E.M. Humphries, D. Balzer, C. Neto, Marine antifouling behavior of lubricant-infused nanowrinkled polymeric surfaces, ACS Appl. Mater. Interfaces 10 (2018) 4173–4182, https://doi.org/10.1021/acsami.7b14736.

[3] M.J. Mosquera, D.M. de los Santos, T. Rivas, P. Sanmartín, B. Silva, New nanomaterials for protecting and consolidating stone, J. Nano Res. 8 (2009) 1–12, https://doi.org/10.4028/www.scientific.net/JNanoR.8.1.

[4] I. Banerjee, R.C. Pangule, R.S. Kane, Antifouling coatings: recent developments in the design of surfaces that prevent fouling by proteins, bacteria, and marine organisms, Adv. Mater. 23 (2011) 690–718, https://doi.org/10.1002/adma.201001215.

[5] J.A. Lichter, M.T. Thompson, M. Delgadillo, T. Nishikawa, M.F. Rubner, K.J. Van Vliet, Substrata mechanical stiffness can regulate adhesion of viable bacteria, Biomacromolecules 9 (2008) 1571–1578, https://doi.org/10.1021/bm701430y.

[6] Woods Hole Oceanographic Institution, Marine fouling and its prevention, U. S. Naval Institute, United States Naval Institute Annapolis, Maryland, Woods Hole, Massachusetts, 1952.

[7] M. Lejars, A. Margaillan, C. Bressy, Fouling release coatings: a nontoxic alternative to biocidal antifouling coatings, Chem. Rev. 112 (2012) 4347–4390, https://doi.org/10.1021/cr200350v.

[8] S.K. Kyei, G. Darko, O. Akaranta, Chemistry and application of emerging ecofriendly antifouling paints: a review, J. Coat. Technol. Res. 17 (2020) 315–332, https://doi.org/10.1007/s11998-019-00294-3.

[9] C.M. Magin, S.P. Cooper, A.B. Brennan, Non-toxic antifouling strategies, Mater. Today 13 (2010) 36–44, https://doi.org/10.1016/S1369-7021(10)70058-4.

[10] S.B. Ulaeto, R. Rajan, J.K. Pancrecious, T.P.D. Rajan, B.C. Pai, Developments in smart anticorrosive coatings with multifunctional characteristics, Prog. Org. Coat. 111 (2017) 294–314, https://doi.org/10.1016/j.porgcoat.2017.06.013.

[11] R. Ciriminna, F.V. Bright, M. Pagliaro, Ecofriendly antifouling marine coatings, ACS Sustain. Chem. Eng. 3 (2015) 559–565, https://doi.org/10.1021/sc500845n.

[12] Y. Lvov, E. Abdullayev, Functional polymer–clay nanotube composites with sustained release of chemical agents, Prog. Polym. Sci. 38 (2013) 1690–1719, https://doi.org/10.1016/j.progpolymsci.2013.05.009.

[13] D. Rawtani, Y.K. Agrawal, Multifarious applications of halloysite nanotubes: a review, Rev. Adv. Mater. Sci. 30 (2012) 282–295.

[14] Y. Fu, W. Wang, L. Zhang, V. Vinokurov, A. Stavitskaya, Y. Lvov, Development of marine antifouling epoxy coating enhanced with clay nanotubes, Materials (2019) 12, https://doi.org/10.3390/ma12244195.

[15] A. Kausar, Review on polymer/halloysite nanotube nanocomposite, Polym. - Plast. Technol. Eng. 57 (2018) 548–564, https://doi.org/10.1080/03602559.2017.1329436.

[16] V. Akbari, F. Najafi, H. Vahabi, M. Jouyandeh, M. Badawi, S. Morisset, M. R. Ganjali, M.R. Saeb, Surface chemistry of halloysite nanotubes controls the curability of low filled epoxy nanocomposites, Prog. Org. Coat. 135 (2019) 555–564, https://doi.org/10.1016/j.porgcoat.2019.06.009.

[17] M. Makaremi, P. Pasbakhsh, G. Cavallaro, G. Lazzara, Y.K. Aw, S.M. Lee, S. Milioto, Effect of morphology and size of halloysite nanotubes on functional pectin bionanocomposites for food packaging applications, ACS Appl. Mater. Interfaces 9 (2017) 17476–17488, https://doi.org/10.1021/acsami.7b04297.

[18] S. Srivastava, A. Pandey, Mechanical behavior and thermal stability of ultrasonically synthesized halloysite-epoxy composite, Compos. Commun. 11 (2019) 39–44, https://doi.org/10.1016/j.coco.2018.11.003.

[19] V. Akbari, M. Jouyandeh, S.M.R. Paran, M.R. Ganjali, H. Abdollahi, H. Vahabi, Z. Ahmadi, K. Formela, A. Esmaeili, A. Mohaddespour, S. Habibzadeh, M.R. Saeb, Effect of surface treatment of halloysite nanotubes (HNTs) on the kinetics of epoxy resin cure with amines, Polymers 12 (2020) 930, https://doi.org/10.3390/polym12040930.

[20] A.V. Ullas, B. Jaiswal, Halloysite nanotubes reinforced epoxy- glass microballoons syntactic foams, Compos. Commun. 21 (2020) 100407, https://doi.org/10.1016/j.coco.2020.100407.

[21] J. Hong, T. Wu, H. Wu, B. Zeng, S. Zeng, T. Chen, X. Wang, Z. Lu, C. Yuan, K. Balaji, D.F.S. Petri, L. Dai, Nanohybrid silver nanoparticles@halloysite nanotubes coated with polyphosphazene for effectively enhancing the fire safety of epoxy resin, Chem. Eng. J. (2020) 127087, https://doi.org/10.1016/j.cej.2020.127087.

[22] M. Jouyandeh, F. Tikhani, N. Hampp, D. Akbarzadeh Yazdi, P. Zarrintaj, M. Reza Ganjali, M. Reza Saeb, Highly curable self-healing vitrimer-like cellulose-modified halloysite nanotube/epoxy nanocomposite coatings, Chem. Eng. J. 396 (2020) 125196, https://doi.org/10.1016/j.cej.2020.125196.

[23] M. Jouyandeh, Z. Karami, O. Moini Jazani, K. Formela, S.M.R. Paran, A. Jannesari, M.R. Saeb, Curing epoxy resin with anhydride in the presence of halloysite nanotubes: the contradictory effects of filler concentration, Prog. Org. Coat. 126 (2019) 129–135, https://doi.org/10.1016/j.porgcoat.2018.10.007.

[24] H. Vahabi, M. Jouyandeh, M. Cochez, R. Khalili, C. Vagner, M. Ferriol, E. Movahedifar, B. Ramezanzadeh, M. Rostami, Z. Ranjbar, B.S. Hadavand, M. R. Saeb, Short-lasting fire in partially and completely cured epoxy coatings containing expandable graphite and halloysite nanotube additives, Prog. Org. Coat. 123 (2018) 160–167, https://doi.org/10.1016/j.porgcoat.2018.07.014.

[25] S. Kundu, C.S. Davis, T. Long, R. Sharma, A.J. Crosby, Adhesion of nonplanar wrinkled surfaces, J. Polym. Sci. Part B Polym. Phys. 49 (2011) 179–185, https://doi.org/10.1002/polb.22181.

[26] S. Wu, S. Altenried, A. Zogg, F. Zuber, K. Maniura-Weber, Q. Ren, Role of the surface nanoscale roughness of stainless steel on bacterial adhesion and microcolony formation, ACS Omega 3 (2018) 6456–6464, https://doi.org/10.1021/acsomega.8b00769.

[27] W. Orapiriyakul, P.S. Young, L. Damiati, P.M. Tsimbouri, Antibacterial surface modification of titanium implants in orthopaedics, J. Tissue Eng. 9 (2018) 2041731418789838, https://doi.org/10.1177/2041731418789838.

[28] K. Efimenko, J. Finlay, M.E. Callow, J.A. Callow, J. Genzer, Development and testing of hierarchically wrinkled coatings for marine antifouling, ACS Appl. Mater. Interfaces 1 (2009) 1031–1040, https://doi.org/10.1021/am9000562.

[29] C. Xie, H. Guo, W. Zhao, L. Zhang, Environmentally friendly marine antifouling coating based on a synergistic strategy, Langmuir 36 (2020) 2396–2402, https://doi.org/10.1021/acs.langmuir.9b03764.

[30] Q. Xie, C. Ma, C. Liu, J. Ma, G. Zhang, Poly (dimethylsiloxane)-based polyurethane with chemically attached antifoulants for durable marine antibiofouling, ACS Appl. Mater. Interfaces 7 (2015) 21030–21037, https://doi.org/10.1021/acsami.5b07325.

[31] Y. Fu, C. Gong, W. Wang, L. Zhang, E. Ivanov, Y. Lvov, Antifouling thermoplastic composites with maleimide encapsulated in clay nanotubes, ACS Appl. Mater. Interfaces 9 (2017) 30083–30091, https://doi.org/10.1021/acsami.7b09677.

[32] A. Spepi, C. Duce, A. Pedone, D. Presti, J.-G. Rivera, V. Ierardi, M.R. Tiné, Experimental and DFT characterization of halloysite nanotubes loaded with salicylic acid, J. Phys. Chem. C 120 (2016) 26759–26769, https://doi.org/10.1021/acs.jpcc.6b06964.

[33] JOTUN, Technical Data Sheet Penguard HB, (n.d.). ⟨https://www.jotun.com/Datasheets/Download?url=%2FTDS%2FTDS_613_Penguard%20HB_Euk__GB.pdf⟩.

[34] S. Brunauer, P.H. Emmett, E. Teller, Adsorption of gases in multimolecular layers, J. Am. Chem. Soc. 60 (1938) 309–319, https://doi.org/10.1021/ja01269a023.

[35] E.P. Barrett, L.G. Joyner, P.P. Halenda, The determination of pore volume and area distributions in porous substances. I. Computations from Nitrogen isotherms, J. Am. Chem. Soc. 73 (1951) 373–380, https://doi.org/10.1021/ja01145a126.

[36] P. Costa, J.M. Sousa Lobo, Modeling and comparison of dissolution profiles, Eur. J. Pharm. Sci. 13 (2001) 123–133, https://doi.org/10.1016/S0928-0987(01)00095-1.

[37] N.A. Peppas, B. Narasimhan, Mathematical models in drug delivery: how modeling has shaped the way we design new drug delivery systems, J. Control. Release 190 (2014) 75–81, https://doi.org/10.1016/j.jconrel.2014.06.041.

[38] P.L. Ritger, N.A. Peppas, A simple equation for description of solute release II. Fickian and anomalous release from swellable devices, J. Control. Release 5 (1987) 37–42, https://doi.org/10.1016/0168-3659(87)90035-6.

[39] N.A. Peppas, Analysis of Fickian and non-Fickian drug release from polymers, Pharm. Acta Helv. 60 (1985) 110–111.

[40] K. Kosmidis, P. Argyrakis, P. Macheras, A reappraisal of drug release laws using Monte Carlo simulations: the prevalence of the Weibull function, Pharm. Res. 20 (2003) 988–995, https://doi.org/10.1023/A:1024497920145.

[41] V. Papadopoulou, K. Kosmidis, M. Vlachou, P. Macheras, On the use of the Weibull function for the discernment of drug release mechanisms, Int. J. Pharm. 309 (2006) 44–50, https://doi.org/10.1016/j.ijpharm.2005.10.044.

[42] K. Zakowski, M. Narozny, M. Szocinski, K. Darowicki, Influence of water salinity on corrosion risk—The case of the Southern Baltic Sea coast, Environ. Monit. Assess. 186 (2014) 4871–4879, https://doi.org/10.1007/s10661-014-3744-3.

[43] L. Lisuzzo, G. Cavallaro, P. Pasbakhsh, S. Milioto, G. Lazzara, Why does vacuum drive to the loading of halloysite nanotubes? The key role of water confinement, J. Colloid Interface Sci. 547 (2019) 361–369, https://doi.org/10.1016/j.jcis.2019.04.012.

[44] Y.M. Lvov, D.G. Shchukin, H. Möhwald, R.R. Price, Halloysite clay nanotubes for controlled release of protective agents, ACS Nano 2 (2008) 814–820, https://doi.org/10.1021/nn800259q.

[45] E. Abdullayev, A. Joshi, W. Wei, Y. Zhao, Y. Lvov, Enlargement of halloysite clay nanotube lumen by selective etching of aluminum oxide, ACS Nano 6 (2012) 7216–7226, https://doi.org/10.1021/nn302328x.

[46] Y.M. Lvov, M.M. DeVilliers, R.F. Fakhrullin, The application of halloysite tubule nanoclay in drug delivery, Expert Opin. Drug Deliv. 13 (2016) 977–986, https://doi.org/10.1517/17425247.2016.1169271.

[47] E. Joussein, S. Petit, J. Churchman, B. Theng, D. Righi, B. Delvaux, Halloysite clay minerals - A review, 2005. https://doi.org/10.1180/0009855054040180.

[48] D. Tatini, Pluronic/gelatin composites for controlled release of actives, Colloids Surf. B Biointerfaces 135 (2015) 400–407, https://doi.org/10.1016/j.colsurfb.2015.08.002.

[49] B. Zhong, S. Wang, H. Dong, Y. Luo, Z. Jia, X. Zhou, M. Chen, D. Xie, D. Jia, Halloysite tubes as nanocontainers for herbicide and its controlled release in

biodegradable poly(vinyl alcohol)/starch film, J. Agric. Food Chem. 65 (48) (2017) 10445–10451, https://doi.org/10.1021/acs.jafc.7b04220.
[50] G. Cavallaro, G. Lazzara, S. Milioto, F. Parisi, V. Evtugyn, E. Rozhina, R. Fakhrullin, Nanohydrogel formation within the halloysite lumen for triggered and sustained release, ACS Appl. Mater. Interfaces 10 (2018) 8265–8273, https://doi.org/10.1021/acsami.7b19361.
[51] E.G. Bediako, E. Nyankson, D. Dodoo-Arhin, B. Agyei-Tuffour, D. Łukowiec, B. Tomiczek, A. Yaya, J.K. Efavi, Modified halloysite nanoclay as a vehicle for sustained drug delivery, Heliyon 4 (2018) 689, https://doi.org/10.1016/j.heliyon.2018.e00689.
[52] Y. Lvov, W. Wang, L. Zhang, R. Fakhrullin, Halloysite clay nanotubes for loading and sustained release of functional compounds, Adv. Mater. 28 (2016) 1227–1250, https://doi.org/10.1002/adma.201502341.
[53] W. Guo, W. Liu, L. Xu, P. Feng, Y. Zhang, W. Yang, C. Shuai, Halloysite nanotubes loaded with nano silver for the sustained-release of antibacterial polymer nanocomposite scaffolds, J. Mater. Sci. Technol. 46 (2020) 237–247, https://doi.org/10.1016/j.jmst.2019.11.019.
[54] E. Abdullayev, Y. Lvov, Halloysite clay nanotubes as a ceramic "skeleton" for functional biopolymer composites with sustained drug release, J. Mater. Chem. B 1 (2013) 2894–2903, https://doi.org/10.1039/c3tb20059k.
[55] X. Jin, R. Zhang, M. Su, H. Li, X. Yue, D. Qin, Z. Jiang, Functionalization of halloysite nanotubes by enlargement and layer-by-layer assembly for controlled release of the fungicide iodopropynyl butylcarbamate, RSC Adv. 9 (2019) 42062–42070, https://doi.org/10.1039/C9RA07593C.
[56] F.F. Farshad, T.C. Pesacreta, J.D. Garber, S.R. Bikki, A comparison of surface roughness of pipes as measured by two profilometers and atomic force microscopy, Scanning 23 (2001) 241–248, https://doi.org/10.1002/sca.4950230404.
[57] T.S. Meiron, A. Marmur, I.S. Saguy, Contact angle measurement on rough surfaces, J. Colloid Interface Sci. 274 (2) (2004) 637–644, https://doi.org/10.1016/j.jcis.2004.02.036.
[58] F. Rupp, L. Scheideler, J. Geis-Gerstorfer, J. Geis-Gerstorfer, Chem. Eng. Technol. 25 (9) (2002) 877–882, https://doi.org/10.1002/1521-4125(20020910)25:9<877::AID-CEAT877>3.0.CO;2-D.
[59] R.V. Sedev, J.G. Petrov, A.W. Neumann, Effect of swelling of a polymer surface on advancing and receding contact angles, J. Colloid Interface Sci. 180 (1996) 36–42.
[60] C.N.C. Lam, N. Kim, D. Hui, D.Y. Kwok, M.L. Hair, A.W. Neumann, Colloids Surf. A: Physicochem. Eng. Asp. 189 (2001) 256–278, https://doi.org/10.1016/S0927-7757(01)00589-1.
[61] Y. Fu, W.J. Kao, Drug release kinetics and transport mechanisms of non-degradable and degradable polymeric delivery systems, Expert Opin. Drug Deliv. 7 (2010) 429–444, https://doi.org/10.1517/17425241003602259.
[62] L. Lisuzzo, G. Cavallaro, S. Milioto, G. Lazzara, Halloysite nanotubes coated by chitosan for the controlled release of khellin, Polymers 12 (2020) 1766, https://doi.org/10.3390/polym12081766.
[63] S. Leporatti, Halloysite clay nanotubes as nano-bazookas for drug delivery, Polymer International, Wiley, 2017, pp. 1111–1118 ⟨https://onlinelibrary.wiley.com/doi/full/10.1002/pi.5347⟩.
[64] D.S. Kommireddy, S.M. Sriram, Y.M. Lvov, D.K. Mills, Stem cell attachment to layer-by-layer assembled TiO_2 nanoparticle thin films, Biomaterials 27 (2006) 4296–4303, https://doi.org/10.1016/j.biomaterials.2006.03.042.
[65] G. Mishra, M. Mukhopadhyay, Enhanced antifouling performance of halloysite nanotubes (HNTs) blended poly(vinyl chloride) (PVC/HNTs) ultrafiltration membranes: for water treatment, J. Ind. Eng. Chem. 63 (2018) 366–379, https://doi.org/10.1016/j.jiec.2018.02.037.
[66] M.M. Alghamdi, A.A. El-Zahhar, Novel cellulose acetate propionate-halloysite composite membranes with improved permeation flux, salt rejection, and antifouling properties, Polym. Adv. Technol. 31 (2020) 2526–2534, https://doi.org/10.1002/pat.4979.